PHYSICAL REVIEW B

CONDENSED MATTER

THIRD SERIES, VOLUME 50, NUMBER 12 15 SEPTEMBER 1994-II

X-ray-scattering measurements of the transient structure of a driven charge-density wave

E. Sweetland, A. C. Finnefrock, W. J. Podulka, M. Sutton,* and J. D. Brock
School of Applied and Engineering Physics, Cornell University, Ithaca, New York 14853

D. DiCarlo and R. E. Thorne
Laboratory of Atomic and Solid State Physics, Cornell University, Ithaca, New York 14853
(Received 2 March 1994; revised manuscript received 23 May 1994)

We report time-resolved x-ray-scattering measurements of the transient structural response of the sliding $\mathbf{Q}_1$ charge-density wave (CDW) in $NbSe_3$ to a reversal of the driving electric field. The observed time scale characterizing this response at 70 K varies from ~15 msec for driving fields near threshold to ~2 msec for fields well above threshold. The position and time-dependent strain of the CDW is analyzed in terms of a phenomenological equation of motion for the phase of the CDW order parameter. The value of the damping constant, $\gamma = (3.2 \pm 0.7) \times 10^{-19}$ eV sec Å^{-3}, is in excellent agreement with the value determined from transport measurements. As the driving field approaches threshold from above, the line shape becomes bimodal, suggesting that the CDW does not depin throughout the entire sample at one well-defined voltage.

I. INTRODUCTION

The fundamental statistical physics describing systems which are so far out of equilibrium that the notion of a partition function is not valid is currently not well understood. Our goal is to study the structural response of very simple systems as they are driven between two distinct steady-state configurations, using time-resolved x-ray scattering. The particular experimental systems we chose to study are the charge-density waves (CDW's) found in quasi-one-dimensional metals. The structure of the pinned CDW state has been measured at high resolution. Theory and experiment are in excellent agreement.[1,2] On the other hand, the dynamics of CDW systems are less well understood, particularly the structural aspects. Although a large number of electronic transport experiments have been performed, the results of these experiments are difficult to interpret in terms of microscopic models and time-resolved structural data are limited and restricted primarily to the $K_{0.3}MO_3$ system.[3,4]

In order to acquire the data, we developed a time-resolved, high-resolution x-ray-scattering system capable of measuring the time-evolution of the structure of the sliding $\mathbf{Q}_1$ charge-density wave in $NbSe_3$ as the direction of the driving electric field is reversed. We are able to interpret our data using an equation of motion for the phase of the CDW order parameter which pertains at low temperatures and at large applied fields.

In the next section of this paper, we review the elementary physics describing CDW's in one-dimensional metals and discuss the structure of both stationary and sliding CDW's. In the third section, we review the standard theory describing x-ray scattering from CDW systems and develop some of the extensions necessary to describe evolving systems. We explicitly solve an equation of motion describing the wave number of the CDW. In the fourth section, we review the details of our $NbSe_3$ samples and our experimental apparatus. In Sec. V, we present our time-resolved x-ray-scattering data. We conclude with a brief discussion of our results and an appendix of mathematical details.

II. CHARGE-DENSITY WAVES

A. The pinned state

In his 1955 solid state text, Peierls demonstrated that an ideal one-dimensional metal crystal is unstable to the formation of a CDW state at low temperatures.[5] In the CDW state, the conduction electron density $\rho_c(x)$ is

given by

$$\rho(x) = \overline{\rho} + \rho_c \cos(Qx + \phi), \tag{1}$$

where $\overline{\rho}$ is the mean conduction electron density, $Q = 2k_F$ is the CDW wave number, ρ_c is the CDW condensate density, and ϕ is the phase. In the presence of the lattice-distortion wave, the position of the jth atom x_j is given by

$$x_j = ja + u\sin(Qja + \phi), \tag{2}$$

where u is the amplitude of the distortion wave and a is the real space lattice constant of the undistorted lattice. The conduction-electron-density wave and the lattice-distortion wave have the same phase ϕ. In the literature, CDW's are frequently characterized by a complex order parameter $\Delta e^{i\phi(x)}$. The amplitude Δ is usually taken to be the energy gap, which is linearly proportional to the amplitude of the lattice-distortion wave. The lattice-distortion wave and the associated conduction-electron-density wave are collectively referred to as a *charge-density wave.*

The properties of CDW systems have been studied extensively during the past 15 years. A large fraction of this research has been devoted to studies of the nonlinear electronic transport exhibited by some CDW systems.[6] This nonlinear transport originates in an incommensurate CDW's ability to slide rigidly through an ideal crystal lattice without friction.[7] Real materials always contain lattice defects or impurities. These localized defects have energetic preferences for the phase and tend to "pin" the CDW in small regions, hence the term "defect pinning."

Two phenomena are associated with defect pinning. First, the system can take advantage of the pinning energy of the defects by elastically distorting the CDW. This elastic distortion can be described by allowing the phase ϕ to become a function of position. Clearly, this positional dependence destroys the long-range periodicity of the CDW state. The *phase-phase* correlation function, $\langle e^{i\phi(\mathbf{x}_1)} e^{-i\phi(\mathbf{x}_2)} \rangle \sim e^{-|\mathbf{x}_1 - \mathbf{x}_2|/\xi}$, is frequently used to describe this loss of long-range periodicity and is characterized by the length scale ξ. A large fraction of the theory of and experiments performed on CDW systems have been devoted to studying this loss of long-range order. Second, and of particular relevance to this experiment, arbitrarily small fields are no longer capable of causing the CDW to slide. The CDW remains pinned until the applied field exceeds a threshold value E_T.[8,9] Experimentally, the onset of sliding is signaled by the presence of a nonohmic contribution to the conductivity when the current exceeds the threshold current I_T.

B. The sliding state, boundary conditions, and phase slip

In any experimental realization, electrical contacts are required to produce the electric field that drives the CDW into the sliding state. The boundary conditions imposed by these electrical contacts play a crucial role in determining the structure of the sliding CDW state. To achieve a steady-state collective current due to the CDW sliding, current must be injected at one electrode and extracted at the other. Equivalently, CDW phase fronts must be added at one electrode and removed at the other. In Fig. 1, the dashed lines indicate lines of constant phase of the CDW. In the region of the sample between the contacts, the CDW phase fronts are moving when the CDW is sliding. In the regions of the sample which are outside the electrical contacts, there is no collective current and the CDW phase fronts are stationary.

This intuitive picture suggests a simple model for the current conversion process originally proposed by Gill to explain the transients observed in his pulsed electronic transport measurements.[10] Consider the contact on the top of Fig. 1. Before the electric field is applied, the CDW is uniform. As the electric field is applied, phase fronts in between the electrodes try to move down, dilating the CDW near the electrode on the top. This strain can be relieved by nucleating a dislocation loop, which quickly grows to be the size of the sample, inserting a new phase front as it does so. This mechanism of nucleating new lines of phase is called *phase slip.*[11]

In electronic transport experiments, the phase-slip mechanism is studied[10,12] in a "transposed" configuration. In the "normal" four-probe configuration, current is injected at the ends of the sample and the voltage is measured at contacts which are separated by a distance L. Measurements[10,12–14] find that, for a given I_{CDW}, there is a difference between the voltage measured in the normal and transposed configurations. This difference is characterized by the phase-slip voltage V_{ps}.

A one-dimensional theory of the steady-state current conversion process has been developed by Ramakrishna *et al.*[15,16] In this theory, the dislocation loops are thermally nucleated in the presence of a background strain field. As in any nucleation and growth problem, loops above a critical size grow and those below the critical size collapse.[17] The resulting equations of motion for $\phi(z,t)$ are linearized and solved for the time-independent com-

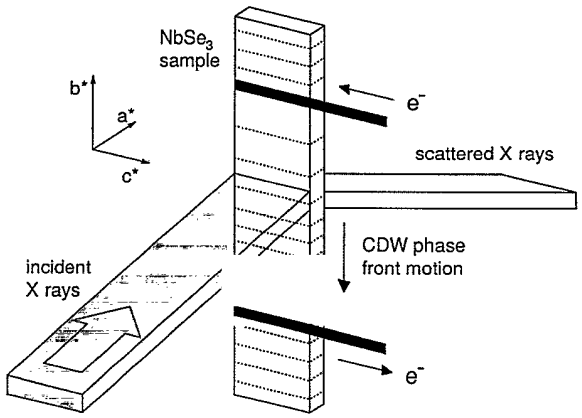

FIG. 1. Schematic illustration of the experimental configuration. Normal current is injected and extracted from the current electrodes. CDW or collective mode conduction takes place only in the region between the current electrodes.

ponent $\phi_1(z)$. The steady-state solution to this model has a parabolic profile and is zero at the electrodes,

$$\phi_1(z) = \frac{-1}{2K_z\Delta^2}\left(\frac{e\rho_c}{2k_F}\right)\left(\frac{V_{ps}}{L}\right)\left[z^2-\left(\frac{L}{2}\right)^2\right]. \quad (3)$$

Here, K_z is the CDW elastic constant and z is the distance from the midpoint between the contacts. The positional dependence of ϕ_1 creates a positional dependence of Q, the CDW wave number. Using synchrotron-based high-resolution x-ray-scattering techniques, DiCarlo *et al.*[18] have observed a position, temperature, and electric field dependent strain of the sliding $\mathbf{Q}_1$ CDW in $NbSe_3$ consistent with the specific predictions of this model. The goal of the present experiments is to measure the time dependence of this strain field as the sign of the electric field is reversed.

III. X-RAY SCATTERING FROM CDW'S

X-ray scattering is a nearly ideal probe of the periodic structure of a CDW. In this section, we will review the standard theory relating the observed x-ray scattering to the microscopic structure of the CDW. Then, we will discuss some extensions necessary to describe time-dependent systems.

A. Kinematic scattering theory

In the kinematic approximation, the scattered intensity measured in an x-ray-scattering experiment is directly proportional to the spatial Fourier transform of the *equal-time* electronic density-density correlation function[19]

$$S(\mathbf{q},t) \propto \int d\mathbf{x}_1 \int d\mathbf{x}_2\, e^{i\mathbf{q}\cdot(\mathbf{x}_1-\mathbf{x}_2)}\langle\rho(\mathbf{x}_1)\rho(\mathbf{x}_2)\rangle_{P(t)}. \quad (4)$$

In this expression, $\mathbf{q}$ is the scattering vector and ρ is the electronic charge density. The angular brackets indicate an ensemble average over all accessible configurations of the system. The subscript $P(t)$ identifies the time-dependent probability distribution to be used when taking this average.

At low temperatures, the electronic charge density of an ideal, monatomic crystal can be approximated by

$$\rho(\mathbf{x}) = \sum_j \rho_A(\mathbf{x}-\mathbf{R}_j), \quad (5)$$

where $\rho_A(\mathbf{x})$ is the electronic charge density of an isolated atom and $\{\mathbf{R}_j\}$ is the set of equilibrium lattice sites. The sinusoidal lattice distortion associated with the CDW state can be introduced by letting

$$\mathbf{R}_j \rightarrow \mathbf{R}_j + \mathbf{u}\sin(\mathbf{Q}\cdot\mathbf{R}_j + \phi(\mathbf{R}_j)). \quad (6)$$

We then proceed to calculate the $T=0$ structure factor, $S(\mathbf{q},t)$, arriving at the expression[20,21]

$$S(\mathbf{q}) \sim |F(\mathbf{q})|^2\Big\{|J_0(\mathbf{q}\cdot\mathbf{u})|^2\sum_j e^{i\mathbf{q}\cdot\mathbf{R}_j} + |J_1(\mathbf{q}\cdot\mathbf{u})|^2 \times \sum_j e^{i(\mathbf{q}\pm\mathbf{Q})\cdot\mathbf{R}_j}\left\langle e^{i[\phi(\mathbf{0})-\phi(\mathbf{R}_j)]}\right\rangle + \cdots\Big\}. \quad (7)$$

Here, $|F(\mathbf{q})|^2$ is the atomic form factor and $J_n(x)$ is the nth order Bessel function and the notation specifying $P(t)$ has been suppressed. The first sum inside the curly brackets produces the Bragg peaks associated with the undistorted crystal lattice. The second sum creates satellite peaks separated by $\pm\mathbf{Q}$ from each Bragg peak. Since this is still a $T=0$ model, the angular brackets in this term indicate an average over different realizations of the quenched defect distribution. The line shape of the CDW satellite peaks is given by the spatial Fourier transform of the *equal-time-phase-phase* correlation function.

In these measurements, $\mathbf{q}\cdot\mathbf{u} \ll 1$ so we can use small argument expansions for the Bessel functions to simplify Eq. (7), producing

$$S(\mathbf{q}) \sim |F(\mathbf{q})|^2\Big\{\sum_j e^{i\mathbf{q}\cdot\mathbf{R}_j} + \tfrac{1}{4}(\mathbf{q}\cdot\mathbf{u})^2\sum_j e^{i(\mathbf{q}\pm\mathbf{Q})\cdot\mathbf{R}_j} \times \left\langle e^{i[\phi(\mathbf{0})-\phi(\mathbf{R}_j)]}\right\rangle + \cdots\Big\}, \quad (8)$$

which exhibits both the necessary Bragg peaks and the q^2 behavior commonly associated with disorder scattering at the CDW satellite positions.

Note that the x-ray measurements are dominated by the localized atomic core electrons. These x-ray-scattering experiments on CDW systems probe the structure of the lattice-distortion-wave component of the CDW state. The conduction-electron-density wave plays only an incidental role in determining the form of the observed scattering.

B. X-ray-scattering theory for evolving systems

In principle, one would like to analyze the data using an expression containing the full $S(\mathbf{q},t)$. Note that, as defined in Eq. (4), the time dependence of $S(\mathbf{q},t)$ originates in the time dependence of the probability distribution $P(t)$. Thus, in a time-dependent measurement, one is studying the evolution of $P(t)$. Frequently, the Fokker-Planck equation is used for such studies. Such an analysis is not out of the question for this system. For example, the elegant formalism developed to study the kinetics of first order phase transitions[22] might be applied to this problem. However, the signal to noise ratio of our data is not yet sufficiently high to warrant such an analysis. Instead, as in the experiments of DiCarlo *et al.*,[18] we will only seek to understand the physics describing the evolution of the strain of the CDW as a function of time and position on the sample. In essence, we will be studying the evolution of the first moment of the probability distribution, not the full distribution function.

As in the steady-state case,[15,16,23] we begin with a Langevin equation of motion for $\phi(\mathbf{r},t)$

$$\gamma\frac{\partial\phi(\mathbf{r},t)}{\partial t} = K_z\triangle^2\left(\nabla^2\phi(\mathbf{r},t)\right) + \frac{e\rho_c}{2k_F}E(t) + F_{\rm imp}(\phi) + \eta(\mathbf{r},t). \quad (9)$$

Here γ is a damping constant, $F_{\rm imp}(\phi)$ is the quenched random pinning force, and $\eta(\mathbf{r},t)$ is the Langevin noise field. The model of Ref. 15 divides ϕ into two components: $\phi = \phi_0 + \phi_1$. Here, ϕ_0 represents the solution to the sliding CDW problem in an infinite sample and ϕ_1 is a small correction that describes the effects of the current contacts and is assumed to vary slowly in time and space. After substituting the decomposition into Eq. (9), the resulting equation is averaged over impurities, time, and space. ac conductivity measurements[6] on $NbSe_3$ find that the natural frequency of the CDW is on the order of 10 MHz. As shown below, the characteristic time scale for changes in ϕ_1 is on the order of 10^{-3} sec. Defining time averages on intervals larger than the period of ϕ_0 but shorter than the characteristic time of ϕ_1 allows one to make connection to the experimentally measured $V_{\rm ps}$. In the limit where the driving electric field is far enough above threshold that the pinning force and the noise term are both negligible, the resulting equation of motion for ϕ_1 is a simple driven diffusion equation,

$$\gamma\frac{\partial\phi_1(z,t)}{\partial t} = K_z\triangle^2\frac{\partial^2\phi_1(z,t)}{\partial z^2} + \left(\frac{e\rho_c}{2k_F}\right)\frac{V_{\rm ps}(t)}{L}. \quad (10)$$

Equation (10) is the time-dependent version of Eq. (8) in Ref. 15.

We are interested in the solution to Eq. (10) for the simple case where the sign of the driving field $V_{\rm ps}(t)$ is reversed at $t = 0$ and $\phi_1(\pm\frac{L}{2}) = 0$. Laplace transform techniques produce a series solution which converges rapidly at early times. Conversely, the separation of variables technique produces a series solution which converges rapidly at late times. The details of the latter series solution are given in the Appendix. Using the appropriate solution at a given time t we have a convenient representation of the solution for all times $t > 0$.

IV. EXPERIMENTAL

A. $NbSe_3$

We chose to use $NbSe_3$ for our experiments for a number of reasons. First, although a large number of materials are known to exhibit CDW states, the CDW's in $NbSe_3$ both exhibit sliding mode conduction and have been extensively studied in electronic transport measurements.[28] Second, we are able to grow crystallographically perfect, single-crystal whiskers of $NbSe_3$. These structural defect-free samples are essential if one wishes to measure these small strains.[18] Third, in $NbSe_3$ the Fermi surface is not completely gapped below the first Peierls transition. The system remains metallic and the electronic transport is still dominated by the normal carriers. Consequently, the electric field must remain uniform inside the whisker, eliminating spurious polarization effects due to poor electrical contacts in regions not too close to the electrodes. Finally, the technology required to produce good electrical contacts has been well developed for $NbSe_3$.

On a microscopic level, the crystal structure of $NbSe_3$ is monoclinic,[24] with lattice constants $a = 10.009$ Å, $b = 3.4805$ Å, $c = 15.629$ Å, and $\beta = 109.47°$. Macroscopically, these crystals grow as long whiskers with a rectangular cross section. The width of a whisker is typically ten times the thickness. Typical dimensions of a sample used in our experiments are on the order of 2 μm $\times$ 20 μm $\times$ 10 mm. Both the crystallographic **b** and **b*** directions are oriented along the whisker axis. The smallest macroscopic sample dimension usually corresponds to the **a*** direction.

Two independent CDW's form in $NbSe_3$. The $\mathbf{Q}_1$ CDW forms at a temperature of $T_{P_1} = 145$ K and has the wave vector[25] $\mathbf{q}_1 = (0\ Q_1\ 0)$, where Q_1 is slightly temperature dependent and approximately equal to 0.243. The $\mathbf{Q}_2$ CDW forms at roughly $T_{P_2} = 59$ K and has the wave vector $\mathbf{q}_2 = (0.5\ Q_2\ 0.5)$, where Q_2 is approximately equal to 0.263. All of the measurements reported in this paper were performed at temperatures above T_{P_2} and below T_{P_1}.

B. Experimental configuration

The x-ray-scattering measurements were performed at the F2 experimental station at the Cornell High Energy Synchrotron Source (CHESS). The storage ring was running at an energy of 5 GeV and the stored positron current typically decayed from 80 to 40 mA during a 50 min fill cycle. For the purposes of comparing different data sets, we have normalized the data to counts per sec at 100-mA ring current. A Si(111) double-bounce monochromator selected a wavelength of 1.5 Å from the white x-ray beam produced by the 24-pole wiggler. A flat Au-coated mirror in the hutch suppressed harmonics of the fundamental wavelength passed by the monochromator. The sagittally bent second monochromator crystal focused the x-ray beam in the out-of-scattering-plane direction at the sample position. Tantalum slits restricted the x-ray spot size at the sample to approximately 0.8 mm $\times$ 3 mm. The resulting x-ray beam contained 4×10^{10} x rays/sec/100 mA of stored positron current. The scattered x rays were analyzed by a triple-bounce channel-cut Si(111) crystal and detected by a standard NaI(Tl) scintillator and photomultiplier tube.

The $NbSe_3$ whiskers were mounted across a 4-mm hole in an alumina substrate using silver paint, which also provided the electrical contacts. The distance between the electrical contacts was $L = 5$ mm. In these measurements the sample was oriented such that the length of the sample in the beam was 0.8 mm, centered at roughly the $\frac{3}{4}$ position between the contacts.

To study the transient structural response of the CDW, we made a stroboscopic measurement.[26] The CDW is subjected to a continuous square wave voltage wave form. The half period of the square wave is divided into time intervals of equal size. X rays detected during a particular

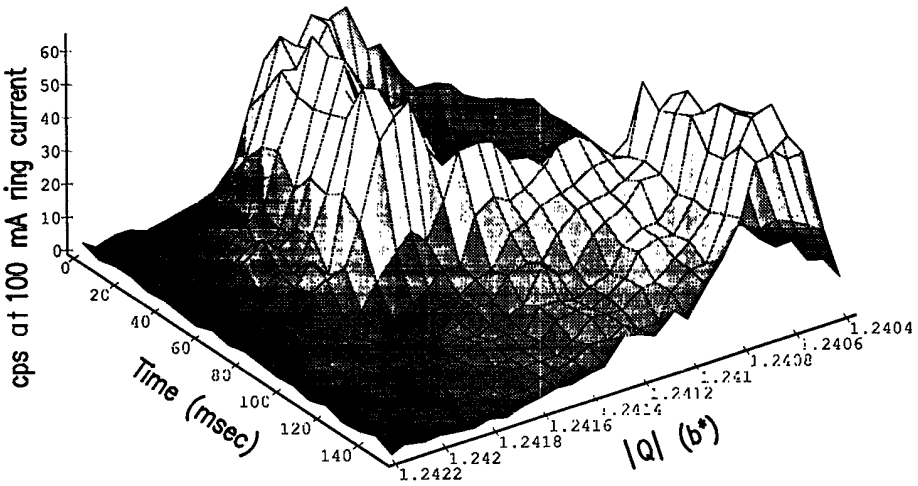

FIG. 2. Scattered intensity measured near the CDW satellite as a function of the scattering vector [0 Q 0] and time t plotted as a two-dimensional surface. This data set was taken at a temperature of 70 K and current of 21 mA. $I_T = 20 \pm 3$ mA. The signal wave form, shown in the inset to Fig. 3, switches polarity at 0 and 80 msec. The time bins are each 8 msec wide.

time interval are summed over a large number of square wave periods. Typical count rates at the CDW satellite were on the order of 50 counts/sec at 100 mA of ring current. Therefore, in order to obtain reasonable counting statistics in a 4 msec wide time bin, we sum over roughly 10 000 voltage wave form cycles. Transient structural effects due to Ohmic heating of the sample were eliminated by switching only the direction of a constant magnitude current, thus keeping the Ohmic heating constant. Time-resolved measurements of the (0 $\overline{2}$ 0) Bragg peak as the current direction is switched do not exhibit any measurable change, ruling out transients due to changes in the lattice (e.g., a strain of the lattice due to a bend of the whisker driven by the electric field).

All the data presented in this paper were taken on the [0 $\overline{1+Q_1}$ 0] CDW satellite. The [0 $\pm(1+Q_1)$ 0] CDW satellites are particularly attractive for high-resolution work because they are nearly nondispersive for Si(111) monochromator-analyzer optics and because the (0 1 0) structure factor is zero in $NbSe_3$, eliminating any diffuse background from the $\frac{1}{q^2}$ tail of the Bragg peak. The measured q-space resolution (full width at half maximum) of our diffractometer in this region of reciprocal space was $\delta q_t = 7.6 \times 10^{-5}$ Å^{-1}, $\delta q_l = 2.7 \times 10^{-4}$ Å^{-1}, and $\delta q_x \sim 1 \times 10^{-2}$ Å^{-1}.

V. EXPERIMENTAL RESULTS

A. Data

All of the data shown in the figures were taken at 70 K. Using the standard technique, the depinning current was measured by using a lock-in amplifier to measure the differential resistance as a function of current. At 90 K, $I_T = 10 \pm 1$ mA. Based on this measurement, we estimate[27] that at 70 K, $I_T = 20 \pm 3$ mA.

Figure 2 illustrates a typical data set: the observed intensity $I(q,t)$ is plotted as a two-dimensional surface. The same data set is also shown in Fig. 3 as a contour plot. The evolution of the CDW satellite as the system is driven by the voltage wave form shown in the inset is clearly visible in either figure. The solid lines in Fig. 3 are contours of constant scattered intensity. The contours are separated by 30 counts/sec at 100 mA. The magnitude of the driving current wave form in this case was 21 mA, slightly greater than the threshold current, $I_T \simeq 20$ mA. After the current direction is switched, a slow shift in the position of the CDW satellite is visible with a time scale on the order of a few msec. The period of the driving wave form is chosen so that the CDW satellite peak stabilizes at its steady-state position before the next switch in the direction of the current.

Close inspection of Figs. 2 and 3 reveals that the satellite peak does not have the same shape or width for the different current directions. The data exhibit several other asymmetric features. In particular, the position

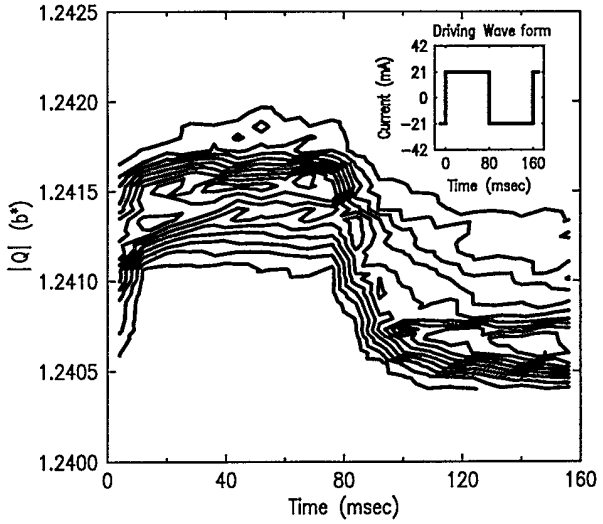

FIG. 3. A contour plot of the same data shown in Fig. 2. The contours are lines of constant scattered intensity. Neighboring contours differ by 30 counts/sec at 100 mA. The highest contour represents a total accumulation of 300 counts in a time bin. The signal wave form, shown in the inset, switches polarity at 0 and 80 msec. The time bins are each 8 msec wide.

and width of the line shape of the zero-field cooled state differ from those of the pinned state which a sliding CDW relaxes into after the driving field is removed. The details of these asymmetries are also position dependent. The asymmetry of the line shape of the driven sliding state is more clearly seen at lower driving fields. For example, Fig. 4 shows a series of longitudinal scans through the CDW satellite from different time intervals as the current direction is switched. These data were taken at 70 K and with a driving current of 17 mA. Each scan is offset by 35 counts/sec at 100 mA for clarity. The top and bottom scans represent the steady state for the two current directions. The remaining scans show that the CDW satellite peak evolves from a single peak to a bimodal line shape. Data sets taken with higher driving current magnitudes exhibited the same systematic structure. In general, as the driving current magnitude was increased, the area under the stationary peak decreased. At 29 mA, the stationary peak is no longer measurable. The width of the moving peak is slightly broader in the transient regions.

To characterize the data, we fit to a two-component line shape. One peak was constrained to have a time-invariant position, width, and integrated intensity. The integrated intensity of the second peak was also held constant, but the position and width were allowed to vary with time. Empirically, each of the peaks is well described by a pseudo-Voigt line shape.[29] The solid lines shown in Fig. 4 represent fits to the sum of two pseudo-Voigt functions. The values of χ^2 for the fits were between 1 and 4 where we have assumed that the errors are due to counting statistics.

Figure 5 displays the fraction of the total integrated intensity under the stationary peak as a function of the magnitude of the driving current. The fraction of the sample which remains pinned decreases monotonically as the current is raised. At a current magnitude of 29 mA, this fraction drops to zero. Due to systematic changes in the scattering geometry as the diffractometer was raised and lowered in order to vary z, we cannot directly compare the intensities observed in different sets.

Figure 6 shows the difference in position of the sliding and pinned peaks as a function of time for one complete period of the driving current wave form. The particular data set shown was taken at a current of 29 mA but is representative of the data taken at all currents. Error bars represent standard fitting errors.[30]

B. Analysis and discussion

A simple interpretation of these data is that at driving fields near the threshold to sliding the CDW breaks into domains. Although a collective current is flowing, some portions of the sample remain unstrained and hence are presumed to be pinned. One possible explanation of the physics is that near an impurity site, the applied electric field may be insufficient to cause the CDW to slide. The same singularity in the dielectric function, $\epsilon(\mathbf{q}, \omega = 0)$, which drives the CDW phase transition also causes the system to respond to a point impurity by creating a localized electronic state[31] with wave number $Q = 2k_F$. Indeed, this second effect is the origin of impurity pinning.

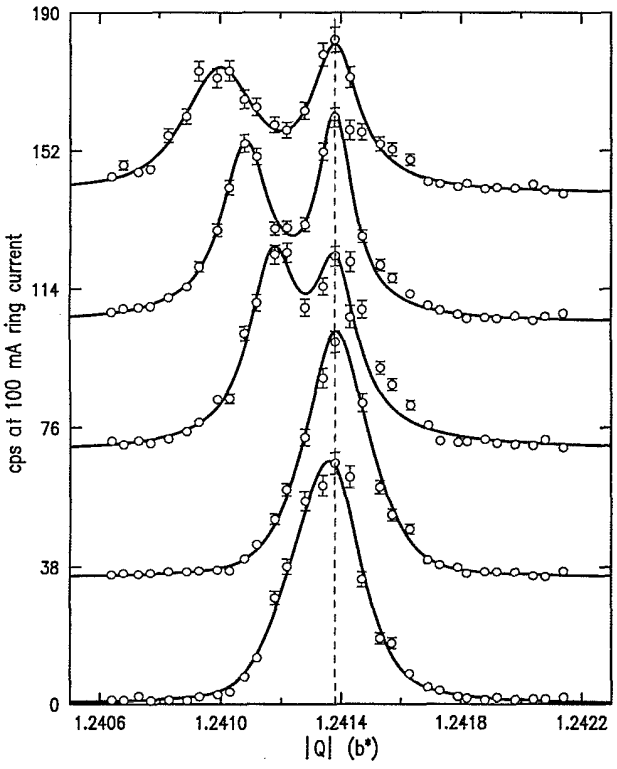

FIG. 4. A succession of (0 Q 0) reciprocal space scans taken from different time slices of a data set taken at 17 mA. Each time bin is 0.004 sec wide. The centers of the time bins, measured from the rising edge of the driving wave form, are 0.014, 0.030, 0.050, 0.062, and 0.078 sec. Successive scans are displaced by 35 counts/sec at 100 mA. The solid lines are the best fit to the sum of two pseudo-Voigt functions, one stationary and the other moving.

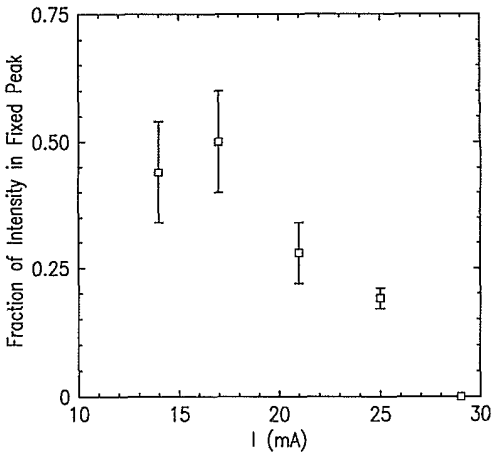

FIG. 5. The ratio of the area under the stationary peak to the total area under the peaks is plotted as a function of current at 70 K. These areas are determined using the two-component pseudo-Voigt line shape demonstrated in Fig. 4. The error bars represent standard fitting errors.

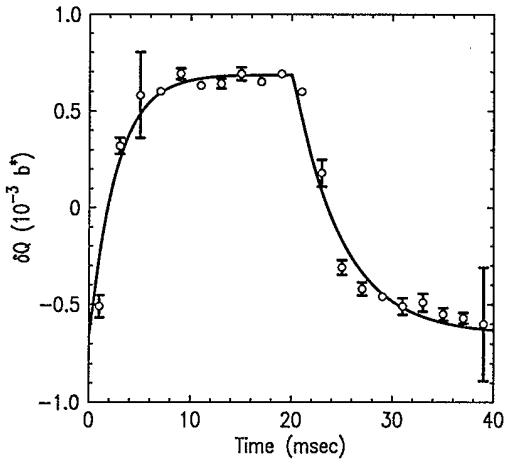

FIG. 6. Positions of the moving peak are shown for a data set taken at a current of 29 mA ($I_T = 20 \pm 3$ mA). The solid lines are the best fit to Eq. (11) in the text.

However, the pinned portions of the sample should not exhibit the time-dependent strain of the sliding portions. Our measurements support this picture. Near threshold, we observe significant broadening of the CDW satellite peak in the $\mathbf{a}^*$ direction. In the $\mathbf{b}^*$ direction, the peak width is roughly 25% greater in the sliding state than in the zero-field cooled state. Further measurements at various temperatures, driving voltages, and wave forms are required to determine these length scales accurately. The observation that increasing the current reduces the area under the stationary peak provides further support for this picture of locally pinned regions since at large enough fields (currents), the whole sample should be in the sliding state. In this scenario, the depinning current measured using the lock-in amplifier cannot be interpreted simply as the single current at which the CDW is depinned over the entire crystal. Rather, our data suggest a picture which is somewhat reminiscent of percolation.

Quantitative analysis of these time-dependent strain results is somewhat problematic. Specifically, Eq. (10) applies only at driving fields well above threshold. The highest current at which we were able to obtain data was on the order of $1.5I_T$. The model specifically predicts that the time constants for different directions should be the same; yet, the data are clearly asymmetric. Furthermore, there are not enough time bins in the transition region to make a reliable test of Eq. (10) and hence the model.

On the other hand, these data are sufficient to demonstrate that x-ray measurements produce results which are consistent with electronic transport measurements. To characterize quantitatively the time scales of the observed transients, we fit the relative peak positions to

$$Q(z,t) = Q_0 \pm \delta Q \left(2e^{-t/\tau_0} - 1\right) \sin\left(\frac{\pi z}{L}\right), \qquad (11)$$

where $\tau_0 = \frac{L^2\gamma}{\pi^2 K_z \Delta^2}$. This equation describing the transient structural response is the derivative of Eq. (A8) in the Appendix. The solid line in Fig. (6) is the best fit to Eq. (11). The amplitude, δQ, and the nominal zero-field value Q_0 were forced to be consistent for the current switch in both directions but the time constant τ_0 was allowed to differ. For the $I = 29$ mA data set shown in Fig. 6, the time constant τ_0 obtained for the switch to larger values of Q was 2.6 ± 0.4 msec and for the switch to smaller values of Q was 4.7 ± 0.7 msec. Using the latter value of τ_0, Eq. (A9) and $K_z\Delta^2 = (1.7 \pm 0.25) \times 10^{-2}$ eV Å^{-1},[18] the value of γ becomes $(3.2 \pm 0.7) \times 10^{-19}$ eV sec A^{-3}.

This value of γ can be compared directly to the value γ obtained from the high-field CDW conductance using the relation

$$\gamma = \left(\frac{\rho_c e}{2k_F}\right)^2 \frac{1}{\sigma_{\rm CDW}}. \qquad (12)$$

Using the values $\sigma_{\rm CDW} = 2 \times 10^5\ \Omega^{-1}\,{\rm m}^{-1}$ and $\rho_c = 3.8 \times 10^{27}\,{\rm m}^{-3}$ appropriate for $NbSe_3$, we find that $\gamma = 5.7 \times 10^{-19}$ eV sec Å^{-3}, in excellent agreement with the x-ray estimate.

The time constants obtained as a function of driving current amplitude are shown in Fig. 7. Error bars again represent standard fitting errors. For current magnitudes ≥ 17 mA there is a monotonic decrease in τ_0 as the current magnitude increases. For $I = 14$ mA, however, there is a jump to shorter time scales, comparable to those observed at 29 mA. Similarly, the magnitude of the strain is much smaller. We do not have an explanation for this behavior but observe that this jump occurs at roughly the depinning current. It is possible that at currents below the depinning current, the CDW is "sloshing" back and forth slightly as hypothesized by Feinberg and Freidel.[32]

VI. SUMMARY AND CONCLUSIONS

In summary, we have developed a time-resolved high-resolution x-ray-scattering system capable of measuring

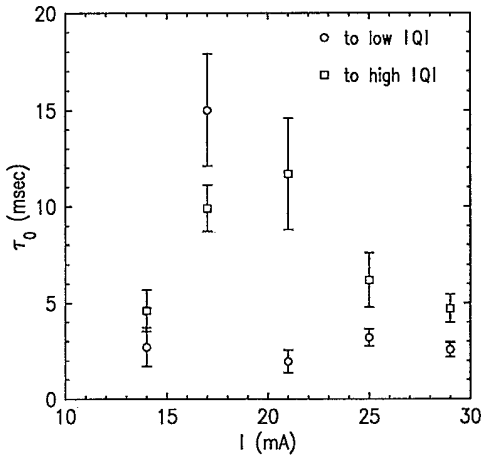

FIG. 7. The characteristic time constants τ_0 derived from fits such as those shown in Fig. 6 are shown as a function of current. Empirically, the time constants to approach the different current directions are not the same. For $I \geq 20$ mA, the values of τ_0 decrease monotonically with increasing current.

the transient structural response of a simple quasi-one-dimensional CDW system as it is driven between two distinct steady-state configurations. We find that a simple Langevin equation of motion for the phase of the CDW, which is based on the notion of a background strain which is driving the nucleation of dislocation loops, gives a value of the phenomenological damping constant γ for the $\mathbf{Q}_1$ CDW in $NbSe_3$ of $(3.2 \pm 0.7) \times 10^{-19}$ eV sec Å^{-3}. This value of γ is in excellent agreement with the value obtained from electronic transport experiments. As the driving field approaches threshold from above, the line shape becomes bimodal and the area under the stationary component of the line shape increases monotonically. This suggests that the CDW did not depin throughout the entire sample at one well-defined voltage. Clearly, much more work needs to be done. In particular, experiments addressing the asymmetry in the response of the sample and simultaneous electronic transport measurements need to be performed. However, these preliminary x-ray measurements demonstrate the potential of the technique for studying kinetics in CDW systems.

ACKNOWLEDGMENTS

The authors thank S. Ramakrishna, J. Sethna, C. Meyers, S. Coppersmith, and P. Littlewood for stimulating discussions. M.S. acknowledges the hospitality of Cornell's Materials Science Center and School of Applied & Engineering Physics during the 1991-92 academic year. This work was supported by the Materials Science Center (NSF Grant No. DMR-88-1858-A02) and by the NSF (Grant No. DMR-92-57466). Additional support was provided by the AT&T Foundation. CHESS is supported by the NSF (Grant No. DMR-90-21700).

APPENDIX

A series solution to Eq. (10) can be obtained by performing a solution similar to a separation of variables calculation. Equation (10) has the generic form

$$\phi_t = a^2 \phi_{zz} + w(z,t). \tag{A1}$$

We begin by assuming a series solution of the form

$$\phi_1(z,t) = \sum_{n=0}^{\infty} \alpha_n(t) \cos\left(\frac{(2n+1)\pi z}{L}\right), \tag{A2}$$

which both spans the space of functions for $-\frac{L}{2} < z < \frac{L}{2}$ and satisfies the boundary conditions. This solution happens, in this special case, to have the form of a conventional Fourier series.

Substituting this series solution into Eq. (A1) leads to an ordinary differential equation in $\alpha_n(t)$,

$$\alpha_n'(t) = -a^2 \left(\frac{(2n+1)^2\pi^2}{L^2}\right) \alpha_n(t) + w_n(t), \tag{A3}$$

where $w_n(t)$ is the coefficient of the expansion of the driving function $w(z,t)$, i.e.,

$$w(z,t) = \sum_{n=0}^{\infty} w_n(t) \cos\left(\frac{(2n+1)\pi z}{L}\right). \tag{A4}$$

The solution of Eq. (A3) is

$$\begin{aligned} \alpha_n(t) = \exp&\left[-\frac{(2n+1)^2\pi^2 a^2}{L^2} t\right] \\ &\times \left\{ \int_0^t \exp\left[\frac{(2n+1)^2\pi^2 a^2}{L^2}\tau\right] \right. \\ &\left. \times w_n(\tau) d\tau + c_n \right\}. \end{aligned} \tag{A5}$$

To determine the constants of integration c_n, we now use the fact that $\phi(z,0) = f(z)$, i.e.,

$$f(z) = \sum_{n=0}^{\infty} \alpha_n(0) \cos\left(\frac{(2n+1)\pi z}{L}\right) \tag{A6}$$

so that the $c_n = \alpha_n(0)$ are simply the expansion coefficients of the initial state $\phi(z,0)$. For our problem, $w(z,t) = \left(\frac{1}{K_z\Delta^2}\right)\left(\frac{e\rho_c}{2k_F}\right)\left(\frac{V_{ps}}{L}\right)$ and the initial state is given by Eq. (3). Therefore,

$$c_n = -\left(\frac{1}{K_z\Delta^2}\right)\left(\frac{e\rho_c}{2k_F}\right)\frac{4V_{ps}L(-1)^n}{\pi^3(2n+1)^3}. \tag{A7}$$

Thus, using these $\{c_n\}$, the solution for $\phi_1(z,t)$ is

$$\begin{aligned} \phi_1(z,t) &= \sum_{n=0}^{\infty} c_n \left[2e^{-t/\tau_n} - 1\right] \cos\left(\frac{(2n+1)\pi z}{L}\right), \\ &\simeq c_0 \left(2e^{-t/\tau_0} - 1\right) \cos\left(\frac{\pi z}{L}\right), \end{aligned} \tag{A8}$$

where

$$\tau_n = \frac{L^2\gamma}{(2n+1)^2\pi^2 K_z \Delta^2}. \tag{A9}$$

* Permanent address: Department of Physics, McGill University, Montreal, PQ H3A-2T8, Canada.

[1] D. DiCarlo, R.E. Thorne, E. Sweetland, M. Sutton, and J.D. Brock, Phys. Rev. B (to be published).
[2] J.P. Pouget *et al.*, J. Phys. (Paris) Lett. **44**, L113 (1983).
[3] J. Zhang, J.F. Ma, S.E. Nagler, and S.E. Brown, Phys. Rev. Lett. **70**, 3095 (1993).
[4] L. Mihaly, K.B. Lee, and P.W. Stephens, Phys. Rev. B **36**, 1793 (1987).
[5] R.E. Peierls, *Quantum Theory of Solids* (Oxford University, New York, 1955).
[6] For comprehensive reviews of the electronic properties of CDW systems, see P. Monceau, in *Electronic Properties of Quasi-One-Dimensional Materials* (Reidel, Dordrecht,

1985), Pt. II, p. 139; G. Grüner, Rev. Mod. Phys. **60**, 1129 (1988).

[7] H. Fröhlich, Proc. R. Soc. London Ser. A **223**, 296 (1954).

[8] R.M. Fleming and C.C. Grimes, Phys. Rev. Lett. **42**, 1423 (1979).

[9] The argument for a commensurate system is similar; however, one expects E_T to be significantly larger.

[10] J.C. Gill, J. Phys. C **19**, 6589 (1986); Physica (Amsterdam) **143B**, 49 (1986).

[11] For a comprehensive review of previous work on CDW phase slip, see F.Ya. Nad', in *Charge Density Waves in Solids*, edited by L.P. Gor'kov and G. Grüner (Elsevier, Amsterdam, 1989), p. 189.

[12] P. Monceau, M. Renard, J. Richard, and M.C. Saint-Lager, Physica (Amsterdam) **143B**, 64 (1986).

[13] D.V. Borodin, S.V. Zaitsev-Zotov, and F.Ya. Nad', Zh. Eksp. Teor. Fiz. **93**, 1394 (1987) [Sov. Phys. JETP **66**, 793 (1987)].

[14] M. Maher, T.L. Adelman, S. Ramakrishna, J.P. McCarten, D.A. DiCarlo, and R.E. Thorne, Phys. Rev. Lett. **68**, 3084 (1992).

[15] S. Ramakrishna, M.P. Maher, V. Ambegaokar, and U. Eckern, Phys. Rev. Lett. **68**, 2066 (1992). Note that the definition of z used in this paper differs from that used in the present one.

[16] Satish Ramakrishna, Phys. Rev. B **48**, 5025 (1993). Note that the definition of z used in this paper differs from that used in the present one.

[17] E.M. Lifshitz and L.P. Pitaevskii, *Physical Kinetics*, Vol. 10 of the *Landau and Lifshitz Course of Theoretical Physics* (Pergamon Press, New York, 1981).

[18] D.A. DiCarlo, E. Sweetland, M. Sutton, J.D. Brock, and R.E. Thorne, Phys. Rev. Lett. **70**, 845 (1993). Note that the definition of z used in this paper differs from that used in the present one. Similarly, contrary to the present paper, this paper combines K_z and Δ^2 into one variable.

[19] An excellent discussion of kinematic scattering theory is given in W. Marshall and R.D. Lowde, Rep. Prog. Phys. **31**, 705 (1968); W. Marshall and S.W. Lovesy, *Theory of Thermal Neutron Scattering* (Oxford University, New York, 1971).

[20] A.W. Overhauser, Phys. Rev. B **3**, 3173 (1971).

[21] The key algebraic transformation in this derivation is the use of the Jacobi-Anger generating function for Bessel functions: $e^{ix\sin\theta} = \sum_n e^{in\theta} J_n(x)$.

[22] J.S. Langer, in *Solids Far From Equilibrium*, edited by C. Godrèche (Cambridge University Press, New York, 1992).

[23] U. Eckern and S. Ramakrishna, Phys. Rev. B **44**, 984 (1991).

[24] J.L. Hodeau, M. Marezio, C. Roucau, R. Ayroles, A. Meerschaut, J. Rouxel, and P. Monceau, J. Phys. C **11**, 4117 (1978).

[25] A.H. Moudden, J.D. Axe, P. Monceau, and F. Levy, Phys. Rev. Lett. **65**, 223 (1990).

[26] Similar techniques have been used to study $K_{0.3}MoO_3$. See, for example, T. Tamegai, K. Tsutsumi, and S. Kagoshima, Synth. Met. **19**, 923 (1987), and references therein.

[27] J. McCarten, M. Maher, T.L. Adelman, D.A. DiCarlo, and R.E. Thorne, Phys. Rev. B. **43**, 6800 (1991).

[28] S. Kagoshima, H. Nagasawa, and T. Sambongi, *One-Dimensional Conductors* (Springer-Verlag, New York, 1988).

[29] A pseudo-Voigt function is the sum of a Lorentzian and a Gaussian. Both peaks are constrained to have the same half width at half maximum (HWHM). The adjustable parameters then become the integrated intensity, the HWHM, the ratio of the two peaks, and the peak position. This line shape was originally proposed as an approximate form of the Voigt line shape which is the convolution of a Lorentzian and a Gaussian. It is particularly useful for obtaining good measures of the HWHM and the integrated intensity when the physical line shape is unknown. See, for example G.K. Wertheim, M.A. Butler, K.W. West, and N.E. Buchanan, Rev. Sci. Instrum. **45**, 1369 (1974).

[30] Philip R. Bevington, *Data Reduction and Error Analysis for the Physical Sciences* (McGraw-Hill, New York, 1969).

[31] J.M. Zimon, *Principles of the Theory of Solids* (Cambridge University Press, New York, 1986), Chap. 5.

[32] D. Feinberg and J. Freidel, in *Low-Dimensional Electronic Properties of Molybdenum Bronzes and Oxides*, edited by C. Schlenker (Kluwer, Dordrecht, 1989), p. 407.